SPE-181480-MS

Novel Method for Evaluating Shale Gas and Shale Tight Oil Reservoirs Using Well Log Data

Robert Freedman[1] and **David Rose**, Schlumberger; and **Boqin Sun**, **Ronald L. Brown, and Thomas Malizia**, Chevron

This paper was prepared for presentation at the SPE Annual Technical Conference and Exhibition held in Dubai, UAE, 26–28 September 2016.

Abstract

This paper introduces a novel method for improved evaluation of shale gas reservoirs, shale tight oil reservoirs, and immature organic shale source rocks. The method provides exact and original algebraic equations for determining total porosities, producible fluid volumes, total hydrocarbon volumes, kerogen volumes, and immobile hydrocarbon volumes. The determination of accurate porosities and fluid volumes in organic shale reservoirs is critical for formation evaluation considering the low porosities (3 to 8 p.u.) typically found in shale reservoirs.

We analyze the challenges associated with interpreting logging tool responses in poor quality shale reservoirs and propose a suite of logging tool measurements that are most likely to overcome the problems. A small set of logging tool measurements (i.e., three or four) that have known responses to fluid and solid volumes and have negligible surface effects were selected. Thus our approach aims to circumvent the interpretation problems caused by poorly understood complex fluid-surface interactions that are exacerbated in shales by high surface-to-volume ratios and clays and other conductive minerals.

The logging tool measurements that we use to predict the shale reservoir properties are bulk densities, nuclear magnetic resonance (NMR) porosities, and total organic carbon (TOC) weight fractions derived from total carbon concentrations measured by a gamma ray spectroscopy tool. The tool response equations for these measurements are written as volume weighted averages of reservoir properties. The producible gas in shale gas reservoirs and the high API gravity producible oils in shale tight oil reservoirs cause the apparent (i.e., measured) NMR porosities to read too low and the apparent density log porosities to read too high. Kerogen also causes the density log porosities to read too high.

The tool response equations are solved simultaneously and exactly to determine shale total porosities, fluid volumes, and kerogen volumes. The solution for the shale total porosity is automatically corrected for light hydrocarbon effects on the density and NMR porosity measurements and for kerogen effects on the density porosities. The exact algebraic solutions or “plug-in formulas” for shale reservoir properties

[1] Retired from Schlumberger, 1 February 2016.

are the main results of the paper. The robustness of these solutions in the presence of measurement noise is studied using Monte Carlo simulations. We discuss the standard deviations of the predicted reservoir properties for different measurement noise levels and the effects of errors in the assumed reservoir fluid and solid properties (e.g., gas density, gas hydrogen index, kerogen density) on the accuracies of the predicted reservoir properties.

The algebraic solutions are used to predict reservoir properties from log data acquired in a shale gas well and a shale tight oil well. The results in both wells are shown to compare favorably with available core data.

Introduction

The steady decline of oil and gas production in North America during the latter part of the 20th century was markedly and unexpectedly reversed by the shale oil and shale gas revolution which coincidentally started at the beginning of the new millennium. This revolution has no doubt changed the worldwide energy balance in the 21st century. The seeds of this revolution were sown in 1982 when the visionary oilman George Mitchell and his company, Mitchell Energy and Development Corp. (MEDC), drilled a vertical exploratory well in north-central Texas to test the gas-producing potential of the Barnett shale (Steward 2007). The MEDC 1-Slay well was not even close to being an economic success but it marked the beginning of a near 20-year effort by MEDC to achieve commercially viable gas production from the Barnett shale. MEDC achieved commercial gas production from Barnett shale wells by the late 1990s and, as a result, established many best practices for drilling, completing, and stimulating shale wells. These practices include advances in horizontal drilling, massive multi-stage fracturing, use of slick water instead of gels for fracturing, the use of microseismic responses for monitoring fracture propagation, and selection of brittle shale zones based on their mineralogy and mechanical properties (Steward 2007; Jarvie et al. 2007). Today, there are numerous prolific shale gas fields (e.g., Barnett shale, Marcellus shale, and Haynesville shale) in North America that were developed following the lead of MEDC. The quest to produce more lucrative liquids (i.e., light oil and gas condensate) in place of natural gas led oil companies to develop prolific shale oil fields (e.g., Eagle Ford, Bakken, and Permian Basin) that produce high API gravity (e.g., 37–43 ^{o}API) light oils. These shale oil resource plays were largely developed following the Barnett shale playbook.

Formation evaluation from well logs was not a major contributor in fostering the shale revolution and there is no doubt that it took a back seat to pressure pumping and horizontal drilling. It was generally assumed that petrophysics rules, cutoffs, and pay criteria used to evaluate logs in conventional formations would not apply to shale reservoirs. This thinking was justified because shale reservoirs have permeabilities in the nanodarcy to microdarcy range, which means that rules for classifying pay in conventional reservoirs based on cutoffs for porosities, water saturations, and net footage are not applicable in shales. The earliest log evaluation work on organic shales was done at a time when shales were considered seals and traps. Organic shales were known to be source rocks in which kerogen was thermogenically transformed, over geological time scales, to hydrocarbons that migrated to and charged nearby conventional reservoirs. This early work on organic shales predated the shale revolution and focused on determining the total organic carbon (TOC). TOC is a measure of organic richness which was primarily of interest to petroleum geochemists and geologists as a means of classifying the hydrocarbon potential of sedimentary basins (e.g., Schmoker 1979; Herron and Le Tendre 1990; Passey et al. 1990). By the beginning of the millennium, the industry recognized that organic shales were not only source rocks for conventional reservoirs but were themselves also producible reservoirs. Once the industry recognized that a huge new petroleum resource was available for exploitation, the intense drilling activity that followed was accompanied by considerable effort to develop techniques for predicting quantitative shale properties from logging tool measurements. These efforts have created a very large body of literature

in the form of industry conference papers, journal papers, and patents devoted to various methods for evaluating well log data in organic shales.

The reservoir properties of interest in the petrophysical evaluation of organic shale reservoirs include mineral fractions, porosities, kerogen volumes, TOC, and hydrocarbon volumes. Additionally, the mechanical properties of the shale reservoir, such as Poisson's ratio, are important for determining the brittleness of the shale in the intervals of interest. Quantitative knowledge of these properties is important for selecting depth intervals containing sweet spots for landing horizontal wells and for the efficient propagation of hydraulic fractures, which are critical for achieving commercial production rates.

Challenges in Shale Formation Evaluation. There are numerous challenges unique to shale petrophysics that must be confronted and solved to determine reliable and robust shale reservoir properties from well logs.

First, the mineral matrix in organic shales is typically a complex mixed lithology containing significant concentrations of many minerals including quartz, calcite, dolomite, clays, micas, feldspars, pyrite, siderite, and anhydrite as well as trace concentrations of other minerals (Freedman et al. 2015). The interpretation of many well logging measurements (e.g., dielectric, sonic, neutron, and density) requires knowledge of physical properties of the mineral matrix. For example, to determine porosity from bulk density log measurements, one must know the dry mineral matrix density (ρ_{ma}), which requires knowledge of the dry weight mineral concentrations.

Second, three types of porosity contribute to the total porosity in organic shales. These are intergranular, intraparticle, and organic matter (OM) porosity. The OM porosity is created during the transformation of kerogen to hydrocarbons, which leaves holes or OM porosity in the remaining kerogen (Loucks et al. 2012). The plant and animal organic remains that are eventually transformed into kerogen were originally deposited together with the inorganic sediments in oceans, streams, and lakes. After many millions of years of burial at increasingly greater depths and exposure to increasingly higher temperatures and pressures, the organic matter is transformed into kerogen, a solid organic material, which is interspersed with the inorganic sediments that constitute the shale mineral matrix (Tissot and Welte 1984, p. 69–92).

Third, several fluid types can occupy the porosity. These include clay-bound and free water, bitumen and immobile oil, and producible light hydrocarbon. The kinds of hydrocarbon fluids, if any, that are present depend on the level of maturity of the kerogen. This is determined by the thermal maturity of the shale, which is commonly characterized by the vitrinite reflectance coefficient (R_o) (Tissot and Welte 1984; Passey et. al. 2010). The vitrinite reflectance coefficient is the percentage of an incident polarized light beam reflected from a kerogen sample immersed in oil. It can be measured in the laboratory on organic shale core samples. The vitrinite reflectance coefficient can be correlated with the maximum temperature and the duration to which the kerogen has been exposed to maximum temperature (Tissot and Welte 1984, p. 515–520).

Fourth, organic shales have very small pore and grain sizes. Inter/intraparticle pore sizes range from about 10 to 3000 nm and OM pores from 5 to 500 nm (Loucks et al. 2012) which means the pores have very high surface-to-volume ratios which significantly enhance surface effects on log measurements of dielectric permittivity, resistivity, and nuclear magnetic resonance (NMR) relaxation times. Complex surface effects can dominate these measurements in shales and can lead to incorrect interpretations.

Fifth, organic shale reservoirs have low porosities typically in the 3- to 8-p.u. range, which reduce the signal-to-noise ratios (SNRs) of some well logging measurements, for example, NMR porosities and relaxation times. Low SNR measurements degrade the precisions of the predicted reservoir properties.

Sixth, the prediction of the volumes of the various fluids that can be present in organic shale reservoirs is more challenging than in conventional reservoirs, where the effects of molecular diffusion on NMR relaxation times measurements acquired with different echo times can be used to compute fluid volumes (Freedman and Heaton 2004). In organic shales, diffusion-based fluid typing is not a viable approach because (1) molecular diffusion is highly restricted in organic shales due to their very small pores and (2) very short surface-induced and bulk-fluid (e.g., clay-bound water and bitumen) relaxation times of the order of milliseconds or less reduce the sensitivity to molecular diffusion. Recent laboratory work (Ozen and Sigal 2013; Tinni et al. 2014) suggests that differences in T_1/T_2 ratios of brine, bitumen and/or immobile oil, and light oil in organic shales can be used for fluid typing in shale tight oil reservoirs. Anand et al. (2015) discuss new NMR logging sequences for more robustly measuring T_1, T_2, and NMR porosity in shales and apply the T_1/T_2 ratios measured in a heavy oil reservoir to estimate oil volumes. The use of T_1/T_2 ratios for fluid typing in organic shales offers promise; however, the method needs further laboratory validation and field testing to establish its robustness and reliability.

The preceding discussion suggests that to develop a robust and reliable log analysis method for organic shales, one should, to the extent possible, avoid using logging tool measurements that are strongly dependent on complex fluid-surface interactions. This led us to consider using a primary suite of logging measurements consisting of bulk densities, NMR porosities, and TOC weight fractions. The response functions for these measurements can be written as volume weighted averages expressed in terms of the reservoir properties. This approach, for these measurements, is based on fundamental petrophysical principles that should apply in both conventional and unconventional reservoirs.

Our paper proposes a simple and transparent new methodology for evaluating shale reservoirs and derives exact algebraic equations, from a selected suite of logging tool responses, for determining shale porosities, kerogen volumes, and hydrocarbon volumes. The reservoir properties are determined from density log porosities, NMR porosities, and TOC measurements and are fully corrected for both kerogen and light-hydrocarbon effects. The methodology and equations are applicable to shale gas, shale tight oil, and immature organic shale source rocks.

The correction for light hydrocarbons and kerogen is necessary to obtain valid results (e.g., see Appendix A). It is well known (e.g., see Passey et al. 2010) that kerogen causes density log porosities to read too high. The producible light oil in shale tight oil reservoirs and the producible gas in shale gas reservoirs cause apparent density log porosities to read too high and apparent NMR log porosities to read too low. Thus, it is not correct to use a standalone porosity tool, such as NMR, to determine the shale porosity and then use that porosity to predict a water saturation from, for example, Archie's equation. To determine accurate shale porosities in shale gas and tight oil reservoirs, it is necessary that the porosities and the fluid volumes be determined simultaneously.

This paper is organized as follows. The Petrophysical Models and Log Responses for Organic Shales section discusses various physical models for organic shales at different stages of thermal maturity and writes the petrophysical response functions in shale gas reservoirs for the primary suite of logging measurements discussed above. The same equations, with obvious changes in fluid properties, are also applicable to shale tight oil reservoirs and immature shale source rocks. This section also discusses the solution of the response equations and derives exact algebraic solutions to these equations that can be used to evaluate organic shale reservoirs and source rocks. These solutions are the main results of this paper. The Field Examples section discusses the application of the algebraic solutions to the prediction of

reservoir properties in a shale gas well and a shale tight oil well and compares the results with available core data. Appendix A discusses the effects of light hydrocarbons on the apparent density and NMR log porosities as well as the effects of kerogen on the density log porosities. Appendix B discusses the effects of measurement noise on the precisions of reservoir properties predicted from the algebraic solutions. Appendix C discusses the errors in the predicted reservoir properties caused by uncertainties in reservoir fluid and solid input parameters.

Petrophysical Models and Log Responses for Organic Shales

The primary logging suite includes bulk density, NMR, and gamma ray spectroscopy tools. The log measurements that are used as inputs to the algebraic equations that determine the reservoir properties are density log porosities, NMR log total porosities, dry weight TOC fractions, matrix densities, and water volumes. In mature shale gas reservoirs that have no bitumen and/or immobile hydrocarbons, water volumes are outputs of the equations and, therefore, do not need to be provided. The gamma ray spectroscopy tool provides dry weight TOC (Radtke et al. 2012) and matrix densities (Freedman et al. 2015). The attractive feature of these particular measurements is that their response functions are simple volume weighted averages. We expect these volumetric relationships to remain valid in shales in contrast to measurements (e.g., resistivity, dielectric) that are affected or dominated by complex surface interactions which are less well understood and predictable.

The first step in constructing petrophysical models for organic shales is to understand the fluids that can be present at different levels of thermal maturity. In organic shale reservoirs, kerogen is always present, and typical kerogen volumetric fractions vary from approximately 0.02 to 0.10. The vitrinite reflectance coefficient (Ro) is a measure of the thermal maturity of the kerogen and determines the types of hydrocarbons that are likely to be present in organic-rich shales. The relationship between Ro, level of maturity, and types of hydrocarbons in a mature organic shale is shown schematically in **Fig. 1**. **Fig. 2** shows a physical model for an immature organic shale (100% water saturation) before the kerogen has started its transformation into bitumen (e.g., Green River shale in the western United States). **Fig. 3** shows a model for a mature organic shale oil reservoir that produces high API gravity oil (e.g., Eagle Ford shale in south Texas, and Bakken shale in North Dakota). Note that immobile oil that has not yet been thermally cracked into light oil can also be present. **Fig. 4** shows a very mature shale gas reservoir having a very high vitrinite reflectance. This reservoir is so far into the gas window that no bitumen and/or immobile hydrocarbons remain in the reservoir. The red dots in the kerogen represent OM porosity (i.e., holes that are filled with free and possibly adsorbed gas). Scanning electron microscope images show that a wide distribution of organic pore sizes exists in kerogen samples from mature reservoirs (Passey et al. 2010).

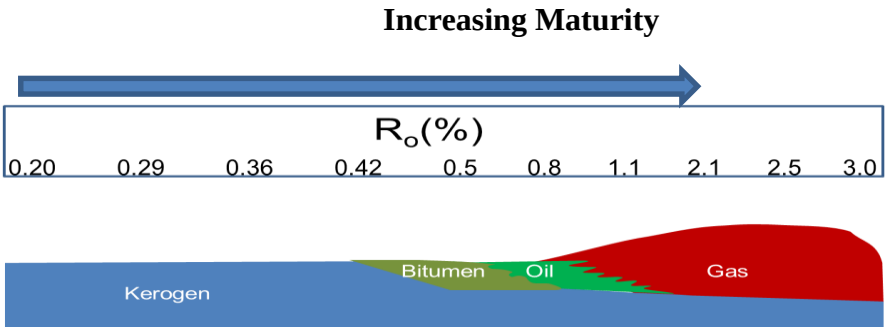

Fig. 1— A qualitative picture of the relationship between the vitrinite reflectance coefficient (R_o) in the top panel and the organic matter in an organic shale reservoir at different levels of thermal maturity characterized by R_o. Note that the reflectance intervals are only approximate, there are no sharp boundaries, and the scale can vary, depending on the type of kerogen (Tissot and Welte 1984, p. 516–519).

Fig. 2— A schematic representation of an immature organic shale source rock. The porosity is 100% water filled. Note that kerogen is not considered part of the porosity. The brine includes all water both clay-bound and free.

Fig. 3— A schematic representation of an organic shale tight oil reservoir. The three fluids that occupy the total porosity are brine, high-gravity producible oil, and bitumen and/or immobile oil.

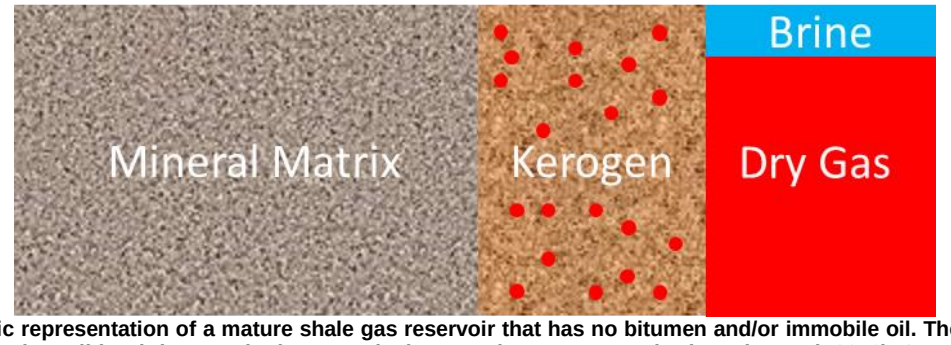

Fig. 4— A schematic representation of a mature shale gas reservoir that has no bitumen and/or immobile oil. The porosity contains only brine and gas. The solid red dots on the kerogen depict organic matter porosity (Loucks et al. 2012). Some of the gas can be adsorbed onto the walls of the organic matter porosity. Note that shale gas reservoirs that are less mature may also contain immobile oil in addition to gas and brine.

Response Functions for Bulk Density, NMR Porosity, and Dry Weight TOC Measurements. Recalling the above models, the response functions for the shale bulk density measurement (ρ_b) and NMR total porosity (ϕ_{nmr}) in a shale gas reservoir can be written as volume weighted averages of the densities of the reservoir solids, liquids, and gas,

$$\rho_b = (1-\phi-V_k)\rho_{ma} + \rho_k V_k + \rho_f(\phi-\phi_g) + \rho_g\phi_g\,, \tag{1}$$

and

$$\phi_{nmr} = \phi_g HI_g + (\phi-\phi_g)HI_f\,. \tag{2}$$

In Eq. 1, we have defined the total shale porosity (ϕ), which includes all fluid-filled pore space (e.g., intergranular, intraparticle, and OM porosities). The quantity V_k is the volume of kerogen in the shale. The factor in parenthesis that multiplies the dry mineral matrix density (ρ_{ma}) in Eq. 1 is the matrix volume. The kerogen density (ρ_k) depends on the type and maturity of the kerogen and is generally in the approximate range from 1.1 to 1.4 g/cm^3 (Okiongbo et al. 2005). In the third term ($\phi-\phi_g$) is the volume

of all fluids (e.g., brine, bitumen, and immobile hydrocarbons) in the porosity other than producible or free gas. The immobile hydrocarbons include immobile gas that can be adsorbed onto the surfaces of the OM pores. The fluid density (ρ_f) is a weighted average of the brine, bitumen, and immobile hydrocarbon densities. Note in Eqs. 1 and 2, the gas is separated from the other fluids (brine, bitumen, and immobile oil) which are described as a single composite fluid. This is sensible because the hydrogen indices (HIs) and densities of the other fluids are similar (e.g., close to those of water). It is the reduced HIs and densities of gas (or high API gravity oils), compared to those of water, that decrease the apparent (measured) bulk densities and the apparent NMR porosities. It is exactly these effects that enable the estimation of gas volumes and producible oil volumes in shale reservoirs. The last term in Eq. 1 is the density of the free or producible gas in the shale where ϕ_g is the volume of producible gas and ρ_g the gas density, which depends on the pressure and temperature of the reservoir. The response function for the NMR total porosity measurement (ϕ_{nmr}) in Eq. 2 is a volume weighted average of the HIs of the fluids and the gas. The HIs in Eq. 2 are the densities of hydrogen nuclei in the reservoir fluids relative to the density of hydrogen nuclei in a tool calibration water sample measured in the laboratory. The HIs in Eq. 2 are not related to, and should not be confused with, the HIs defined in the pyrolysis method used for source rock characterization (Tissot and Welte 1984, p. 509). In Eq. 2, observe that there is no contribution to the NMR porosity from the solid organic matter because the relaxation times of the hydrogen nuclei in solid kerogen are too short to be detected by present-day NMR logging tools. In Eq. 2, we assume that the NMR polarization time is sufficiently long to polarize the gas nuclei. If this is not the case, a polarization factor can be included in the first term of Eq. 2 (Freedman et al. 1998).

The dry weight TOC measurement is derived from the total organic carbon measurement made by a gamma ray spectroscopy tool (Radtke et al. 2012). The response function follows from the definition of this measurement and can be expressed as

$$TOC = \frac{c_k \rho_k V_k + c_{im} \rho_{im} \phi_{im} + c_g \rho_g \phi_g}{\rho_{ma}(1 - V_k - \phi)}, \tag{3}$$

where c_k , c_{im} , and c_g are the fractional weight of carbon in kerogen, immobile oil, and gas, respectively, and ϕ_{im} is the volume of all immobile fluids. The value of c_k varies with the type of kerogen and its maturity and is typically close to 0.8 (Tissot and Welte 1984, p. 141). Similarly, the fractional weight of carbon in crude oils varies depending on the composition of the oil and a value close to 0.84 for c_{im} is reasonable. The value of c_g for methane is 0.75 and for ethane it is 0.8. The denominator in Eq. 3 is the mass of the dry matrix. TOC defined in Eq. 3 is the mass of organic carbon in the shale divided by the mass of the dry mineral matrix. Eq. 3 is consistent with the definition of dry weight TOC derived from the spectroscopy tool (Radtke et al. 2012). It differs from the definition of TOC in the laboratory, which is the mass of organic carbon in the shale divided by the total mass of the sample. In the laboratory definition of TOC, the denominator in Eq. 3 is replaced by the bulk density (ρ_b) of the sample. The volumes in Eq. 3 are related by the constraint equation,

$$\phi = \phi_w + \phi_{im} + \phi_g, \tag{3a}$$

where ϕ_w is the total volume of water and includes both clay-bound and free water. The response equations above are for shale gas reservoirs. The response equations for shale tight oil reservoirs are identical if one replaces shale gas reservoir parameters $c_g, \rho_g, \phi_g, HI_g$ with $c_o, \rho_o, \phi_o, HI_o$, where c_o is the fractional weight

of carbon in the producible light oil, ρ_o is the density of the light oil, ϕ_o is the volume of the light oil, and HI_o is the HI of the light oil.

Solution of the Response Equations. In this section we show that Eqs. 1–3 and Eq. 3a can be solved self-consistently and exactly. The procedure is sequential, and one first solves Eqs. 1 and 2 for ϕ and ϕ_g. One finds after some algebra that the total porosity of the shale gas is given by

$$\phi = w \cdot (DPHI - \lambda_2 V_k) + (1-w) \cdot \frac{\phi_{nmr}}{HI_f}, \tag{4}$$

where we have defined the weight as

$$w = \frac{1 - \frac{HI_g}{HI_f}}{(1 - \frac{HI_g}{HI_f}) + \lambda}, \tag{4a}$$

and the parameters as

$$\lambda = \frac{\rho_f - \rho_g}{\rho_{ma} - \rho_f}, \tag{4b}$$

and

$$\lambda_2 = \frac{\rho_{ma} - \rho_k}{\rho_{ma} - \rho_f}, \tag{4c}$$

and we introduced the density log porosity (DPHI) defined by

$$DPHI = \frac{\rho_{ma} - \rho_b}{\rho_{ma} - \rho_f}. \tag{4d}$$

Eq. 4 is an exact solution of Eqs. 1 and 2 for ϕ, and it provides some useful insights. Observe that the total porosity in Eq. 4 depends on the volume of kerogen which remains to be determined. Also note that the total porosity in Eq. 4 is a weighted sum of the "density log porosity corrected for kerogen" and total NMR porosity divided by HI_f. The weighting factor (w) is given in Eq. 4a. The parameter λ_2 in Eq. 4c provides a kerogen correction to DPHI, which reads too high in organic rich shales because of the low kerogen density (ρ_k) relative to the matrix density (ρ_{ma}). The parameter λ in Eq. 4b provides a light hydrocarbon correction for gas (or for high gravity oil in shale tight oil reservoirs), which causes DPHI to read too high. The shale porosity in Eq. 4 is corrected for both kerogen and light hydrocarbon effects on the density log porosity and for the reduced HI of gas (or of light oil in a shale oil reservoir), which causes ϕ_{nmr} to read too low (see Appendix A). The solution of Eqs. 1 and 2 for the volume of gas ϕ_g is given by

$$\phi_g = \frac{(DPHI - \lambda_2 V_k) - \frac{\phi_{nmr}}{HI_f}}{(1 - \frac{HI_g}{HI_f}) + \lambda}. \tag{5}$$

It can be seen from Eq. 5 that one should require the condition

$$(DPHI - \lambda_2 \cdot V_k) \geq \frac{\phi_{nmr}}{HI_f}. \tag{6}$$

When the above condition is not satisfied, then $\phi < \phi_{nmr} / HI_f$, which is petrophysically incorrect, and $\phi_g < 0$, which is non-physical, as can be seen from Eqs. 4 and 5, respectively. Therefore, if Eq. 6 is not satisfied, one should set $\phi_g = 0$ and $\phi = \phi_{nmr} / HI_f$. Observe that the gas volume in Eq. 5 also depends on the volume of kerogen, which remains to be determined. It is also useful to observe that if $V_k = 0$, then Eqs. 4 and 5 reduce to the analogous density-magnetic resonance (DMR) equations that are industry standards for the evaluation of gas- and light-oil producing conventional reservoirs (Freedman et al. 1998).

To proceed with the simultaneous solutions of Eqs. 1 through 3 and Eq. 3a, one must solve for the kerogen volume (V_k). This can be done by solving Eqs. 3 and 3a. One finds after some straightforward algebra, that V_k is a linear function of the total shale porosity:

$$V_k = A + B \cdot \phi \ , \tag{7}$$

where the coefficients are given by

$$A = \frac{\rho_{ma} \cdot TOC + \phi_g(0) \cdot (c_{im}\rho_{im} - c_g\rho_g) + c_{im}\rho_{im}\phi_w}{\rho_{ma} \cdot TOC + a(c_{im}\rho_{im} - c_g\rho_g) + c_k\rho_k}, \tag{8}$$

and

$$B = -\frac{\rho_{ma}TOC + c_{im}\rho_{im}}{\rho_{ma} \cdot TOC + a(c_{im}\rho_{im} - c_g\rho_g) + c_k\rho_k} \ , \tag{9}$$

where, in arriving at Eqs. 8 and 9, to save space, we found it convenient to define the two quantities:

$$\phi_g(0) = \frac{DPHI - \frac{\phi_{nmr}}{HI_f}}{(1 - \frac{HI_g}{HI_f}) + \lambda}, \tag{10}$$

and

$$a = \frac{\lambda_2}{(1 - \frac{HI_g}{HI_f}) + \lambda} \ . \tag{11}$$

A few observations will provide some insights into Eqs. 7–9. First, note that the coefficients A and B do not depend on the kerogen volume. Also, observe from Eq. 9 that $B < 0$ so that the kerogen volume in Eq. 7 decreases with increasing ϕ. More importantly, A and B depend only on log measurements (i.e., TOC, DPHI, and ϕ_{nmr}), quantities derived from log measurements (i.e., ρ_{ma} and ϕ_w), and user inputs for reservoir fluid and solid properties (e.g., ρ_g, ρ_f, ρ_k, HI_g, HI_f, c_g). Observe that the volume of water

(ϕ_w) in the organic shale is an input that appears in the numerator of Eq. 8 for the coefficient A. There is no generally accepted industry method for determining ϕ_w in organic shale reservoirs. The possible methods include resistivity, dielectric, and the use of cutoffs on NMR relaxation time distributions to separate the water signal from the other fluids. All of these techniques have known limitations. For the purposes of this paper, we recommend the use of one or more of the aforementioned methods supported by core data when available. In the special case of a mature shale gas reservoir (e.g., see Fig. 4) that is known from core analysis to have no bitumen and/or immobile oil, the above equations simplify, and ϕ_w is not a required input, but instead becomes one of the predicted reservoir properties.

On substituting Eq. 7 into Eq. 4 and solving for the gas and kerogen-corrected total porosity of the shale gas reservoir one finds

$$\phi = \frac{(1-\frac{HI_g}{HI_f})\cdot(DPHI-\lambda_2 A)+\lambda\frac{\phi_{nmr}}{HI_f}}{(1-\frac{HI_g}{HI_f})\cdot(1+\lambda_2 B)+\lambda}. \tag{12}$$

As noted earlier in the paragraph following Eq. 3a, the equations derived for shale gas reservoirs in this paper are also valid for tight oil reservoirs if the gas parameters are replaced by those of the tight oil. Equation 12 is a key result of this paper. It is an exact solution of the organic shale petrophysical equations Eqs. 1 through 3 and Eq. 3a. Eq. 12 determines the total shale porosity (ϕ), fully corrected for light hydrocarbon and kerogen effects on the log measurements. The computation of the shale reservoir properties follows sequentially by first computing ϕ from Eq. 12 and then computing V_k from Eq. 7. Next, one uses V_k in Eq. 5 to compute ϕ_g. Finally, the volume of immobile oil can be computed from the equation

$$\phi_{im} = \max(0, \phi - \phi_w - \phi_g). \tag{13}$$

Readers can easily verify that the solutions in Eqs. 12, 7, 5, and 13 exactly satisfy the response equations by considering a particular shale reservoir (i.e., by specifying ϕ, ϕ_g, V_k, ϕ_{im} and specific properties for the fluids and solids in the reservoir), and using Eqs. 1–3 to compute the tool responses. On substituting the tool responses and the specific reservoir fluid and solid properties sequentially into the solutions given in Eqs. 12, 7, 5, and 3a, one finds exact values for the specified formation properties.

Solutions for Immature Source Rocks. The above equations simplify for immature source rocks which, by definition are 100% saturated with brine. One can show that the coefficients *A* and *B* in Eqs. 8 and 9 reduce to

$$A = \frac{\rho_{ma}\cdot TOC}{\rho_{ma}\cdot TOC + c_k\rho_k}, \tag{14}$$

and

$$B = -\frac{\rho_{ma}\cdot TOC}{\rho_{ma}\cdot TOC + c_k\rho_k} \equiv -A. \tag{15}$$

On using these two equations in Eq. 7, one finds that the volume of kerogen in immature source rocks is given by

$$V_{k,sr} = \frac{\rho_{ma} \cdot TOC \cdot (1-\phi)}{\rho_{ma} \cdot TOC + c_k \rho_k}, \tag{16}$$

and Eq. 12 for the porosities in immature rocks reduces to

$$\phi = \frac{\phi_{nmr}}{HI_f}. \tag{17}$$

Thus, the evaluation of porosity, kerogen volume, TOC and matrix mineralogy in immature source rocks requires only an NMR and a gamma ray spectroscopy tool. An alternative and independent expression for the kerogen volume in immature source rocks can be obtained from Eq. 5 by setting the numerator equal to zero, because there are no hydrocarbons, and solving the resulting equation. One finds that

$$V_{k,sr} = \frac{DPHI - \frac{\phi_{nmr}}{HI}}{\lambda_2}. \tag{18}$$

Eqs. 16 and 18 should give comparable results to within measurement errors for the volume of kerogen. However, Eq. 16 is likely to be more robust, especially for low kerogen volumes.

Field Examples

This section uses the algebraic solutions derived in the previous section to evaluate a shale gas well and a shale tight oil well. It is useful to recall the procedure for computing the shale porosities, kerogen volumes, and fluid volumes. One first assigns values to the fluid and solid properties for the shale reservoir and then computes the *A* and *B* coefficients in Eqs. 8 and 9 using the log measurements acquired at each depth. Using the *A* and *B* coefficients one can sequentially compute shale porosities, kerogen volumes, and fluid volumes at each depth using Eqs. 12, 7, 5, and 3a in that order.

Shale Gas Well. The first field example is from a well drilled in the Marcellus shale, which is an organic-rich black shale in the Appalachian Basin of North America. It was formed during the Devonian period and deposited in a deep-water anoxic environment with rich organic matter, which is the source of the gas and oil (Myers 2008) in this formation. Minerals include illite, smectite, chlorite, kaolinite, quartz, K-feldspar, calcite, dolomite, siderite, and pyrite. The porosity ranges from 5 to 9 p.u., water saturations vary between 10 and 40%, and TOC is typically in the range from 2 to 10 wt%. Matrix permeabilities are in the nanodarcy to microdarcy range (Bruner and Smosna 2011).

Fig. 5 shows a logged and cored interval from the Marcellus shale gas well. The open hole logging suite included bulk density, NMR, and gamma ray spectroscopy logs. Core porosities were measured using the water immersion porosimetry (WIP) technique (Kuila et al 2014). TOC from LECO carbon analysis was performed on the cores. Track 1 shows the lithology of the logged interval. Track 2 shows dry weight TOC from the gamma ray spectroscopy tool and core TOC corrected to the same dry weight ratio reference as the gamma ray spectroscopy tool. Track 3 shows the dry weight matrix (or grain) density derived from the spectroscopy tool. Track 3 also shows the bulk density (RHOZ), neutron porosity (TNPH), and NMR total porosity (TCMR) logs. Tracks 4–6 show the shale porosities, kerogen volumes, and fluid volumes computed from the algebraic equations. Note the generally favorable agreement between predicted porosities and kerogen volumes with the core measurements. Track 7 shows water volumes (i.e., $\phi - \phi_g$) computed from the porosities and gas volumes in tracks 4 and 6, respectively. Water volumes are computed outputs in this well because it is drilled in a mature shale gas reservoir that does not contain bitumen and/or immobile oil.

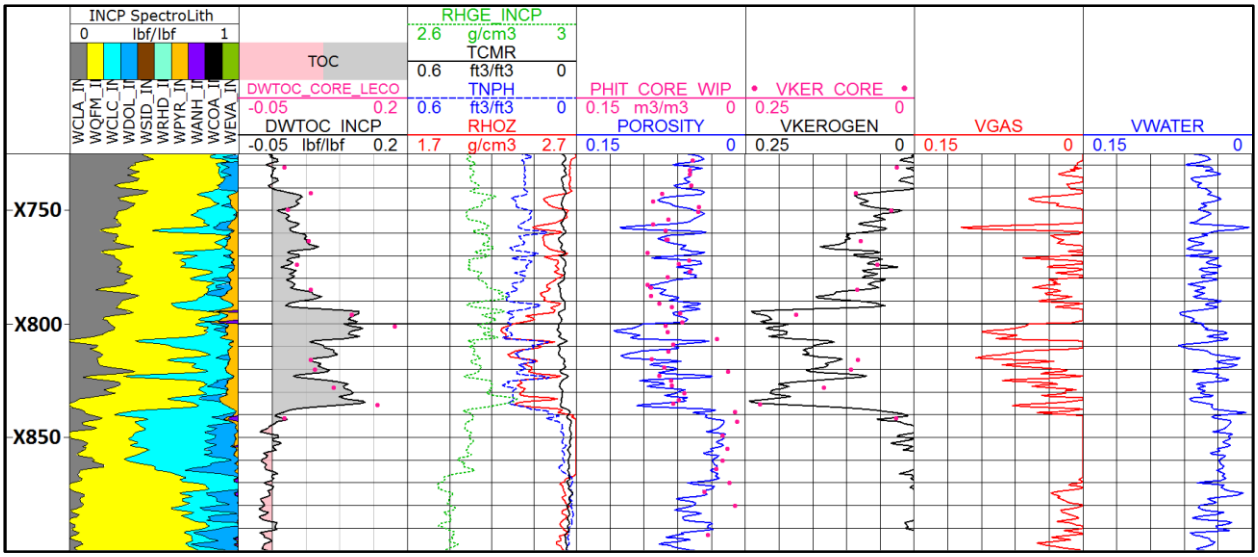

Fig. 5— Evaluation of a shale gas well from the Marcellus shale in the northeast United States. Observe that log-derived shale porosities and kerogen volumes in tracks 4 and 5 are in good overall agreement with the core measured values. The log-derived volumes of gas and water are shown in tracks 6 and 7.

Shale Tight Oil Well. The second example is from a shale tight oil well drilled in the Midland basin in West Texas. The lithology is very complex and contains carbonate and massive mudrock (Handford 1981). The two major stratigraphic sections are the Spraberry/Dean and the Wolfcamp formations. The Spraberry and Dean formations are a series of Leonardian-aged shales with interbedded sands that were associated with channel systems and submarine fans. The Spraberry formation is further divided into upper and lower sandy units above the Dean formation. The Wolfcamp formation is a system of mostly shale with interbedded carbonate (mainly limestone). Minor layers of calcareous sandstone are present. Pore systems in these formations are dominated by micrometer and nanometer size pores with natural fractures. The porosity is typically less than 10 p.u., and the matrix permeability is in the microdarcy range. The key petrophysical challenges include the evaluation of porosities, fluid volumes, matrix permeabilities, and mechanical properties for predicting fracture propagation. The significant local lithological variability of the Wolfcamp formation also makes identifying the correct landing target a major challenge.

Fig. 6 shows an interval from a tight oil well drilled through both the Spraberry/Dean and the Wolfcamp formations. The open-hole logging suite includes gamma ray spectroscopy, bulk density, NMR, and dielectric tools. Core data are available over two intervals in the well. The upper cored interval covers the Lower Spraberry and extends into the Upper Dean, and the lower cored interval covers the Wolfcamp. Tracks 1 and 2 show the lithology, dry weight TOC, and core TOC from LECO corrected to the same dry weight ratio reference as the spectroscopy tool. Track 3 shows the dry weight matrix density from the gamma ray spectroscopy tool. Track 3 also contains bulk density (RHOZ), neutron porosity (TNPH), and NMR total porosity (TCMR) logs. Tracks 4–5 show the porosities, kerogen volumes and total hydrocarbon volumes. The volumes of producible oil and immobile oil computed in this well have poor statistical precisions because of low sensitivities and low measurement signal-to-noise ratios and are not shown here. The low sensitivities are caused by insufficient contrast in the density and HI of the producible oil with the densities and HIs of the other fluids. The effects of low sensitivity and measurement noise on the standard deviations of the producible oil are discussed in detail in Appendix B.

The porosities and kerogen volumes in tracks 4 and 5 computed from the algebraic equations agree well with the core results. The total hydrocarbon volumes in track 6 also compare favorably with volumes of oil measured on cores by Dean-Stark analysis. Track 7 shows water volumes computed from the dielectric tool, which were also used as inputs to the algebraic equations in this case, and compared with water volumes measured by Dean-Stark analysis. Note that the water volumes from the dielectric tool are

consistently higher than the core measured water volumes. Accurate and robust measurement of water volumes from either cores or logs remains a challenge in shale reservoirs. The laboratory measurement of fluids in cores from shale tight oil reservoirs poses numerous challenges and is a subject of current research (Handwerger et al. 2011). Likewise, predictions of water volumes from dielectric or resistivity log measurements can be compromised by simple interpretation models that inadequately account for complex fluid-surface interactions and pore geometry effects.

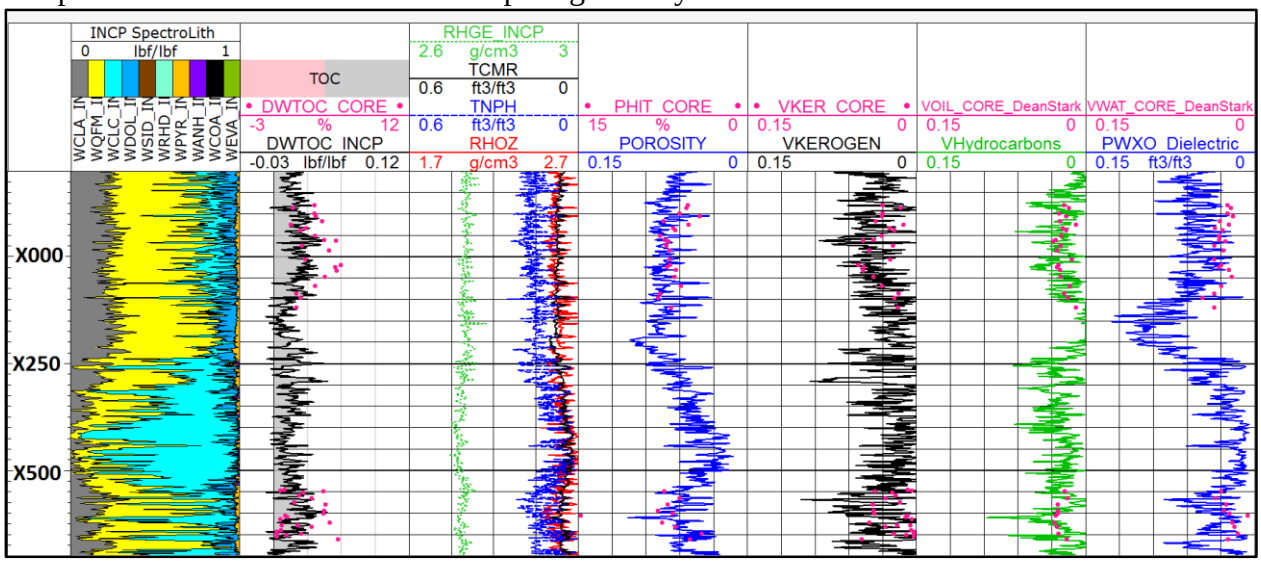

Fig. 6—Evaluation of a shale tight oil well from the Permian Basin in West Texas. The porosities, kerogen volumes, and total hydrocarbon volumes in tracks 4, 5, and 6 are seen to compare well with the core data over both the Spraberry (upper) and Wolfcamp (lower) cored intervals.

Summary and Conclusions

This paper presents a new method for the evaluation of organic shale reservoirs and source rocks. The primary measurements required are density porosity, NMR porosity, and TOC. The TOC measurement is derived from measurements made by a gamma ray spectroscopy tool. In tight oil or gas reservoirs with bitumen and/or immobile oil, the method requires an estimate of water volumes. For mature shale gas reservoirs that have no bitumen or immobile oil, the reservoir water volumes are an output of the method. We derived exact algebraic solutions to the response equations for the primary measurements. The response equations are simple volume weighted averages of the reservoir properties. The exact algebraic solutions of the response equations can be used to estimate total porosities, fluid volumes, and kerogen volumes in shale gas and shale oil reservoirs. The porosities, and therefore the estimated fluid volumes, are automatically corrected for light hydrocarbon effects on density and NMR log porosities and for kerogen effects on density log porosities.

Appendix A discusses light hydrocarbon and kerogen effects on density and NMR log porosities and shows that they are significant and must be accounted for to determine accurate shale porosities, fluid volumes, and kerogen volumes. Appendix B discusses the effects of different levels of tool measurement noise on the precision of predicted reservoir properties. The effects of measurement noise are studied by adding Gaussian noise to the noise-free tool responses. Monte Carlo simulations were done for two shale gas reservoirs and one tight oil reservoir with specified reservoir properties. The results of the simulations are the standard deviations of the estimated shale reservoir properties. The simulations were done using four different tool measurement noise levels, e.g., abnormally high, normal, low, and very low, defined in Appendix B. The conclusions from the Monte Carlo simulations are summarized as follows:

- Porosities and kerogen volumes in shale gas and shale oil reservoirs can be robustly predicted under normal noise levels.

- Gas volumes in shale gas reservoirs can be robustly predicted under normal noise levels.
- Total hydrocarbon volumes in shale gas and shale oil reservoirs can be robustly predicted under normal noise levels.
- Producible light oil volumes in shale oil reservoirs cannot be robustly predicted under normal noise levels, however, they can be robustly predicted under very low noise levels.

The terminology "robustly predicted" is used above to indicate that the standard deviations of the estimated volumes are 1.0 p.u. or less. In mature shale gas reservoirs, with no bitumen or immobile oil, the Monte Carlo simulations show that water volumes can be predicted with standard deviations of approximately 1.3 p.u.

Appendix C discusses errors in the estimated reservoir properties caused by uncertainties in the fluid and solid reservoir properties (e.g., $c_k, c_g, c_o, \rho_k, \rho_g, \rho_o$). The examples in Appendix C show that the predicted reservoir properties are only weakly sensitive to errors in the input parameters. That is, the errors have relatively minor effects on the reservoir properties and do not significantly change the overall evaluation. This relatively weak sensitivity to input parameters has also been observed with field data we have processed to date.

The new method was tested in a shale gas well and in a shale oil well. The predicted reservoir properties were in good overall agreement with the core results in both wells. The field test results were also consistent with our expectations and with the findings and conclusions in the appendices.

Nomenclature

a = used in the definitions of the coefficients A and B and defined in Eq. 11
A = coefficient defined in Eq. 8 and used in determining the shale porosities (Eq. 12) and kerogen volumes (Eq. 7)
B = coefficient defined in Eq. 9 and used in determining the shale porosities (Eq. 12) and kerogen volumes (Eq. 7)
c_g = fractional weight of carbon in the reservoir gas
c_{im} = fractional weight of carbon in the reservoir bitumen and/or immobile oil
c_k = fractional weight of carbon in the reservoir kerogen
c_o = fractional weight of carbon in the reservoir tight oil
DPHI = density log porosity defined in Eq. 4d
HI_g = hydrogen index of the producible gas in shale gas reservoir
HI_f = average hydrogen index of brine, bitumen, and immobile hydrocarbons (default value, $HI_f = 1$) in shale reservoir
HI_o = hydrogen index of the light oil in shale tight oil reservoir
R_o = vitrinite reflection coefficient (%) of kerogen
S_g = gas saturation
S_{im} = bitumen and/or immobile hydrocarbon saturation
w = weight used in Eq. 4 and defined in Eq. 4a
TOC = dry weight total organic carbon measured by the gamma ray spectroscopy logging tool (see Eq. 3)
V_k = volume fraction of kerogen in organic shale reservoirs and source rocks (see Eq. 7)
$V_{k,sr}$ = volume fraction of kerogen in immature source rocks (see Eqs. 16 and 18)
V_{ma} = volume fraction of dry mineral matrix

Δ(DPHI) = shift in density log porosity caused by light hydrocarbons and kerogen (see Eq. A-3)
$\Delta\phi_{nmr}$ = shift in NMR porosity caused by light hydrocarbons (see Eq. A-1)
λ = parameter defined in Eq. 4b that determines the light hydrocarbon effect on DPHI
λ_2 = parameter defined in Eq. 4c that determines the kerogen effect on DPHI
ρ_b = bulk density of shale measured by a density logging tool
ρ_f = fluid density or average of brine, bitumen, and/or immobile hydrocarbon densities (default value, ρ_f = 1 g/cm^3)
ρ_g = density of producible (free) gas in shale gas reservoir
ρ_{im} = average density of bitumen and/or immobile hydrocarbon in organic shale reservoir
ρ_o = density of producible oil in shale tight oil reservoir
ρ_k = density of kerogen in organic shale reservoir or source rock
ρ_{ma} = density of dry mineral matrix in organic shale reservoir or source rock
$\sigma(\phi)$ = standard deviation of shale porosities estimated from Monte Carlo simulations
$\sigma(\phi_g)$ = standard deviation of gas volumes estimated from Monte Carlo simulations
$\sigma(\phi_{hy})$ = standard deviation of total hydrocarbon volumes estimated from Monte Carlo simulations
$\sigma(\phi_{im})$ = standard deviation of bitumen and immobile hydrocarbon volumes estimated from Monte Carlo simulations
$\sigma(\phi_o)$ = standard deviation of producible oil volumes estimated from Monte Carlo simulations
$\sigma(V_k)$ = standard deviation of kerogen volumes estimated from Monte Carlo simulations
ϕ = porosity in organic shale reservoirs and source rocks (see Eq. 12)
ϕ_g = volume of producible (free) gas in shale gas reservoir
$\phi_g(0)$ = used in the definition of the coefficient *A* and defined in Eq. (10)
ϕ_{hc} = volume of light hydrocarbon in shale gas or shale tight oil reservoir (used in Appendix A)
ϕ_{hy} = total volume of hydrocarbons in organic shale reservoir
ϕ_{im} = volume of bitumen and/or immobile hydrocarbons in organic shale reservoir
ϕ_{nmr} = total shale porosity measured by an NMR logging tool
ϕ_o = volume of producible oil in shale tight oil reservoir
ϕ_w = volume of water in a shale reservoir or immature shale source rock

Acknowledgments

We owe thanks to Chevron and Schlumberger management for permission to publish this paper. We thank Michel Claverie for a critical reading of an earlier version of the paper and for suggestions that improved the paper.

References

Anand, V., Ali, M. R., Al-Adani, N. et al. 2015. New Generation NMR Tool for Robust, Continuous T1 and T2 Measurements. Presented at the SPWLA 56th Annual Logging Symposium, Long Beach, California, USA, 18–22 July. SPWLA-2015-CC.

Bruner, K. R. and Smosna, R. 2011. A Comparative Study of the Mississippian Barnett Shale, Fort Worth Basin, and Devonian Marcellus Shale, Appalachian Basin. U.S. Department of Energy DOE/NETL-2011/1478.

Freedman, R. and Heaton, N. 2004. Fluid Characterization Using Nuclear Magnetic Resonance Logging, *Petrophysics* **45** (3): 241–250.

Freedman, R., Herron, S., Anand, V. et al. 2015. New Method for Determining Mineralogy and Matrix Properties from Elemental Chemistry Measured by Gamma Ray Spectroscopy Logging Tools, *SPE Res Eval & Eng* **18** (4): 599–608. SPE-170722-PA http://dx.doi.org/10.2118/170722-PA

Freedman, R., Minh, C. C., Gubelin, G. et al. 1998. Combining NMR and Density Logs for Petrophysical Analysis in Gas-Bearing Formations. Presented at the. SPWLA 39th Annual Logging Symposium, Keystone, Colorado, USA, 26–29 May. Paper II.

Handford, C. R. 1981. Sedimentology and Genetic Stratigraphy of Dean and Spraberry Formations (Permian), Midland Basin, Texas. *AAPG Bulletin* **65** (9): 1602–1616. http://dx.doi.org/10.1306/03b5962a-16d1-11d7-8645000102c1865d.

Handwerger, D.A., Suarez-Rivera, R., Vaughn, K.I. et al. 2011. Improved Petrophysical Core Measurements on Tight Shale Reservoirs Using Retort and Crushed Samples. Presented at the SPE Annual Technical Conference and Exhibition, Denver, Colorado, USA, 30 October–2 November. SPE 147456. http://dx.doi.org/10.2118/147456.

Herron, S. L. and Le Tendre, L. 1990. A Total Organic Carbon Log for Source Rock Evaluation. *AAPG Studies in Geology no. 30, Deposition of Organic Facies*, 57–71Tulsa: AAPG.

Jarvie, D. M., Hill, R. J., Ruble, T. E. et al. 2007. Unconventional Shale-Gas Systems: The Mississippian Barnett Shale of North-Central Texas as One Model for Thermogenic Shale-Gas Assessment. *AAPG Bulletin* **91** (4): 475–499. http://dx.doi.org/10.1306/12190606068

Kuila, U., McCarty, D. K., Derkowski, A. et al. 2014. Total Porosity Measurement in Gas Shales by the Water Immersion Porosimetry (WIP) Method. *Fuel* **117**: 1115–1129. http://dx.doi.org/10.1016/j.fuel.2013.09.073.

Loucks, R. L., Reed, R. M., Ruppel, S. C. et al. 2012. Spectrum of Pore Types and Networks in Mudrocks and a Descriptive Classification for Matrix-Related Mudrock Pores. *AAPG Bulletin* **96** (6): 1071 –1098. http://dx.doi.org/10.1306/08171111061

Myers, R 2008. Marcellus Shale Update. *Independent Oil & Gas Association of West Virginia*.

Okiongbo, Kenneth S., Aplin, Andrew C., and Larter, Steve, R. 2005. Changes in Type II Kerogen Density as a Function of Maturity: Evidence from the Kimmeridge Clay Formation. *Energy & Fuels* **19:** 2495–2499.

Ozen A. E. and Sigal, R. F. 2013. T1/T2 NMR Surface Relaxation Ratio for Hydrocarbons and Brines in Contact with Mature Organic-Shale Reservoir Rocks. *Petrophysics* **54** (1): 11–19.

Passey, Q.R., Creaney, S., Kulla, J. B. et al. 1990. A Practical Model for Organic Richness from Porosity and Resistivity Logs. *The American Association of Petroleum Geologists Bulletin* **74** (12): 1777–1794.

Passey, Q. R., Bohacs, K.M., Esch, W.L. et al. 2010. From Oil-Prone Source Rock to Gas-Producing Shale Reservoir—Geologic and Petrophysical Characterization of Unconventional Shale Gas Reservoirs. Presented at the CPS/SPE International Oil & Gas Conference and Exhibition, Beijing, China, 8–10 June. SPE-131350-MS. http://dx.doi.org/10.2118/131350-MS.

Radtke, R. J., Lorente, M., Adolph, B. et al. 2012. A New Capture and Inelastic Spectroscopy Tool Takes Geochemical Logging to the Next Level. Presented at the SPWLA 53rd Annual Logging Symposium, Cartagena, Columbia, 16–20 June. SPWLA-2012-103.

Schmoker, J. W. 1979. Determination of Organic Content of Appalachian Devonian Shales from Formation-Density Logs. *AAPG Bulletin* **63** (9): 1504–1509.

Steward, D. B. 2007. *The Barnett Shale Play: Phoenix of the Fort Worth Basin—A History*, The Fort Worth Geological Society and The North Texas Geological Society.

Tinni, A., Sondergeld, C., and Rai, C. 2014. NMR T1-T2 Response of Moveable and Non-Moveable Fluids in Conventional and Unconventional Rocks. Presented at the International Symposium of the Society of Core Analysts, Avignon, France, 8–11 September. SCA2014-091.

Tissot, B.P. and Welte, D.H. 1984. *Petroleum Formation and Occurrence*, second edition, Springer-Verlag, New York.

Appendix A—Effects of Light Hydrocarbons and Kerogen on Apparent Density and NMR Porosities

This appendix discusses the effects of light hydrocarbons—gas and high API gravity live oils—on the NMR and density log porosities and the effect of kerogen on the density log porosities in organic shale reservoirs. The light hydrocarbon effect is caused by the low HIs and mass densities of light hydrocarbons compared to the other fluids (i.e., brine, bitumen and immobile hydrocarbons). The reduced HI of light hydrocarbons causes apparent NMR log porosities to read too low. The NMR porosity deficit is proportional to the volume of the light hydrocarbon present in the reservoir. The apparent density log porosities read too high in light hydrocarbons, and the porosity overestimation is proportional to the volume of light hydrocarbon present in the reservoir. Kerogen is not measured by present-day NMR tools because the relaxation times of hydrogen in kerogen are too short to be detected. The kerogen, like the light hydrocarbon effect, also causes the density log porosities to read too high. It should be clear that because of the light hydrocarbon and kerogen effects, accurate reservoir porosities cannot be derived from standalone NMR or density log measurements in organic shale reservoirs without corrections for these effects. The magnitude of the light hydrocarbon effects is greater in shale gas reservoirs but can also be significant in shale oil reservoirs. To clarify the magnitude of the light hydrocarbon and kerogen effects, a few cases are discussed in the following paragraphs.

The NMR porosity deficit is proportional to the light hydrocarbon volume and can be computed from Eq. A-1:

$$\Delta\phi_{nmr} = -\phi_{hc}(1 - HI) \tag{A-1}$$

where ϕ_{hc} denotes either the gas or the light oil volume and HI is the hydrogen index of the light hydrocarbon. The negative sign in Eq. A-1 shows that the measured NMR porosities are decreased because the HIs of light hydrocarbons are less than 1. **Table A-1** shows the light hydrocarbon effects on apparent

(i.e., measured) NMR porosities in both shale gas and shale tight oil reservoirs for the true reservoir porosities in column 1, which range from 4 to 8 p.u. and for hydrocarbon volumes in column 2 that correspond to hydrocarbon saturations of 70%. Observe that the shift in the NMR porosity in Eq. A-1 is proportional to the light hydrocarbon volume, and, therefore, the shift is proportional to the product of the light hydrocarbon saturation and the porosity. The apparent NMR porosities are shown in columns 3 and 4. The HIs depend on the molecular composition of the hydrocarbon, reservoir temperature, and reservoir pressure. The HIs shown in columns 3 and 4 for gas and tight oil, respectively, are comparable to the HIs of gas and producible oils commonly found in organic shale reservoirs. Observe that the apparent NMR porosities for the shale gas reservoir underestimate the true reservoir porosities by amounts that range from 1.7 to 3.4 p.u., which are large considering the low porosities of typical shale reservoirs. Apparent NMR porosities in shale tight oil reservoirs underestimate the true reservoir porosities by amounts that range from 0.6 to 1.1 p.u. which, as expected, are smaller deficits than from NMR porosity in shale gas reservoirs, but are still significant given the low porosities.

True Porosities	Hydrocarbon Volumes	NMR Porosities in Shale Gas Reservoirs (HI_g = 0.4)	NMR Porosities in Shale Tight Oil reservoirs (HI_o = 0.8)
4	2.8	2.3	3.4
5	3.5	2.9	4.3
6	4.2	3.5	5.2
7	4.9	4.0	6.0
8	5.6	4.6	6.9

Table A-1— Light hydrocarbon effects on apparent NMR porosities in shale gas and shale tight oil reservoirs.

Light hydrocarbons have densities less than 1 g/cm^3, which causes density log porosities calculated with a fluid density of 1 g/cm^3 to read too high. The shift in density log porosities caused by light hydrocarbons is given by

$$\Delta(\mathrm{DPHI}) = \frac{\phi_{hc}(1-\rho_{hc})}{\rho_{ma}-1} \equiv \lambda\phi_{hc}, \qquad \text{(A-2)}$$

where ρ_{hc} is the density of the light hydrocarbon and ρ_{ma} is the matrix or dry mineral density of the organic shale. **Table A-2** shows the light hydrocarbon effects on apparent density log porosities in typical shale gas and shale tight oil reservoirs. The gas, tight oil, and matrix densities shown in Table A-2 are comparable to those commonly found in organic shale reservoirs. Observe that in the shale gas reservoirs, the uncorrected density log porosities exceed the true porosities by amounts that range from 1.3 to 2.6 p.u. In the tight oil reservoirs, the uncorrected density log porosities exceed the true porosities by amounts ranging from 0.7 to 1.2 p.u., which are less than in the shale gas reservoirs but are still significant. In addition to the light hydrocarbon effects on the density log porosities, the kerogen also causes high apparent density log porosities.

True Porosities	Hydrocarbon Volumes	Density Log Porosities* in Shale Gas Reservoirs (ρ_g = 0.2 g/cm^3)	Density Log Porosities* in Shale Tight Oil Reservoirs (ρ_o = 0.6 g/cm^3)
4	2.8	5.3	4.7
5	3.5	6.6	5.8
6	4.2	8.0	7.0
7	4.9	9.3	8.2
8	5.6	10.6	9.2
*ρ_{ma} = 2.7 g/cm^3			

Table A-2 — Light hydrocarbon effects on apparent density log porosities in shale gas and shale tight oil reservoirs.

The shift in the apparent density log porosities from both light hydrocarbons and kerogen can be shown from Eq. 1 to be given by Eq. A-3:

$$\Delta(\mathrm{DPHI}) = \frac{\phi_{hc}(1-\rho_{hc}) + V_k(\rho_{ma}-\rho_k)}{\rho_{ma}-1} \equiv \lambda\phi_{hc} + \lambda_2 V_k \,, \tag{A-3}$$

which reduces to Eq. A-2 in organic lean shales that have negligible volumes of kerogen. The reason why kerogen causes the apparent density log porosity to be too high is that the kerogen has a low density compared to that of the mineral matrix, and one can see from the numerator of Eq. A-3 that the kerogen effect depends on the difference between the matrix and the kerogen densities. **Table A-3** shows the combined effects of light hydrocarbons and kerogen on apparent density log porosities in shale gas and shale tight oil reservoirs. The results were computed using matrix and kerogen densities of 2.7 g/cm^3 and 1.4 g/cm^3, respectively. A kerogen volume fraction of 0.05 (5 p.u. when expressed as a volume percent) was used in the computations. Comparing the apparent density log porosities in Tables A-2 and A-3, one sees that kerogen can have a much larger effect than light hydrocarbons on apparent density log porosities.

True Porosities	Hydrocarbon Volumes	Density Log Porosities* in Shale Gas Reservoirs (ρ_g = 0.2 g/cm^3)	Density Log Porosities* in Shale Tight Oil Reservoirs (ρ_o = 0.6 g/cm^3)
4	2.8	9.1	8.5
5	3.5	10.5	9.6
6	4.2	11.8	10.8
7	4.9	13.1	12.0
8	5.6	14.5	13.1
* ρ_{ma} = 2.7 g/cm^3, V_k = 5 p.u. , ρ_k = 1.4 g/cm^3			

Table A-3— Light hydrocarbon and kerogen effects on apparent density log porosities in shale gas and shale tight oil reservoirs.

Appendix B—Monte Carlo Simulations

Effects of Measurement Noise on Solutions. There is always random electronic noise on logging tool measurements, and one must consider the effects of noise on the predicted reservoir properties. There are other sources of errors: (1) uncertainties in the assumed reservoir fluid and solid properties, (2) systematic

measurement or tool calibration errors, and (3) the accuracy of the petrophysical models. This section considers the effects of Gaussian noise on the measurements (i.e., ρ_b, ϕ_{nmr}, TOC). Monte Carlo simulations with 1000 trials were conducted by adding zero mean Gaussian noise with standard deviations for each measurement based on their known electronic and statistical characteristics. To illustrate the effects of random measurement noise on the predicted shale reservoir properties, we consider two shale formations and perform simulations for both shale gas and shale tight oil reservoirs. Moreover, the simulations were performed using different noise levels to elucidate the role that measurement noise plays in the challenging interpretation of these low-porosity reservoirs. **Table B-1** shows the formation properties and the fluid and solid properties used in the simulations for shale gas formations. Note that the values for most of the reservoir inputs shown in Table B-1 are close to those found in **Table B-2** for shale tight oil reservoirs where the produced fluid is high API gravity oil. The two exceptions are the mass density and HI (marked in red) which both have higher values for producible tight oil than for gas.

Formations	ϕ (p.u.)	ϕ_g (p.u.)	V_k (p.u.)	ϕ_{im} (p.u.)	ϕ_w (p.u.)
1	6	4	5	1	1
2	5	3	2	0	2

Reservoir Inputs	C_k	C_{im}	C_g	ρ_f	ρ_g	ρ_{im}	ρ_k	HI_g	HI_f	ρ_{ma}
Formation 1	0.80	0.84	0.80	1.0	0.2	1.0	1.4	0.4	1.0	2.7
Formation 2	0.80	0.84	0.80	1.0	0.2	1.0	1.4	0.4	1.0	2.7

Table B-1 — Formation and reservoir fluid and solid inputs used for shale gas simulations.

The sensitivity of the density and NMR porosity measurements to the light hydrocarbon volumes depends on the contrasts in the density and HI of the light hydrocarbon and the other fluids—brine and immobile hydrocarbons. Thus, there will be more sensitivity to gas volumes than to producible oil volumes. In the absence of any noise, this difference in sensitivity would not matter; however, as the measurement noise levels are increased, it becomes more difficult to robustly predict oil volumes than to predict gas volumes. To illustrate the importance of low measurement noise on the robustness of the predicted reservoir properties, the simulations were performed using several different standard deviations for the tool noises, as shown in **Table B-3**. The measurement noise can be reduced, in practice, by logging more slowly and averaging more measurements.

Formation	ϕ (p.u.)	ϕ_o (p.u.)	V_k (p.u.)	ϕ_{im} (p.u.)	ϕ_w (p.u.)
1	6	4	5	1	1

Reservoir Inputs	C_k	C_{im}	C_o	ρ_f	ρ_o	ρ_{im}	ρ_k	HI_o	HI_f	ρ_{ma}
Formation 1	0.80	0.84	0.80	1.0	0.7	1.0	1.4	0.8	1.0	2.7

Table B-2 —Formation and fluid and solid input properties used for shale tight oil simulations. Observe that the density and HI of the producible tight oil are higher than for gas. The values shown for the density and HI of the producible oil in the table are close to those often found in shale tight oil reservoirs. The exact values depend on the reservoir temperature and pressure and the molecular composition of the oil.

Noise Level	$\sigma(\rho_b)$ (g/cm^3)	$\sigma(\phi_{nmr})$ (p.u./100)	$\sigma(TOC)$ (wt%/100)
High (1)	0.02	0.015	0.01
Normal (2)	0.01	0.01	0.005
Low (3)	0.01	0.005	0.005
Very Low (4)	0.002	0.001	0.001

Table B-3 — The different noise levels used for the Monte Carlo simulations are defined by the standard deviations in the logging tool measurements of the bulk density, NMR total porosity, and total organic carbon.

Monte Carlo simulations were performed by adding zero mean pseudo-random Gaussian noise with the standard deviations shown in Table B-3 to the noise-free responses in Eqs. 1–3. One thousand trials were performed for each simulation and the noisy measurements and the reservoir fluid and solid properties were sequentially entered into Eqs. 12, 7, 5, and 3a to predict 1000 values of ϕ, V_k, ϕ_g (or ϕ_o for a tight oil reservoir), and ϕ_{im}. The volume of water (ϕ_w) was assumed known from dielectric or resistivity measurements or from NMR relaxation time distributions. Total hydrocarbon volume (ϕ_{hy})—the sum of the volumes of the producible oil and the immobile hydrocarbons—were also computed by subtracting ϕ_w from ϕ.

Monte Carlo Simulations in Shale Gas Reservoirs. Monte Carlo simulation results for the estimated reservoir properties are shown in **Fig. B-1** for shale gas formation 1 in Table B-1. The simulation in Fig. B-1 was performed using abnormally high tool measurement noises designated as noise 1 in Table B-3. The x-axes of the five tracks show the reservoir properties predicted for each of the 1000 trials. For each trial, the noisy tool response data were input into the algebraic equations. The reservoir properties predicted by the algebraic equations were plotted without constraints, and in some cases, negative values occur. The standard deviations computed from the 1000 trials for each predicted property are shown at the top of each track. The vertical line in each track intersects the x-axis at the mean of the 1000 trials. Observe that the means of the predictions are exactly equal to the true reservoir properties. This occurs because the algebraic equations are exact solutions to the response equations for noise-free measurements, and therefore they give unbiased (i.e., zero mean) estimates for measurements that have zero mean random noise. Observe that the standard deviations for the shale reservoir properties of greatest interest are relatively low (less than 1.8 p.u.), especially considering that the simulation was performed using abnormally high tool measurement noises. For this simulation, and in general, the most robustly predicted properties from the algebraic equations, for both shale gas and shale tight oil reservoirs, are the total porosity and the volume of kerogen. Before proceeding to discuss the other simulations, a few remarks are helpful. Observe for this simulation and for all other simulations discussed in this paper, the standard deviation in the estimate of the total hydrocarbon volume (ϕ_{hy}) is equal to the standard deviation in the porosity (ϕ) because the water volume is assumed constant. Also, note that the standard deviation in the volume of immobile oil is higher than for the other volumes. This happens because ϕ_{im} is computed from differences in fluid volumes (see Eq. 3a) and therefore it follows from statistics of independent (which is only approximately true here) random variables that the variance (i.e., square of the standard deviation) of ϕ_{im} is the sum of the variances in the other fluid volumes.

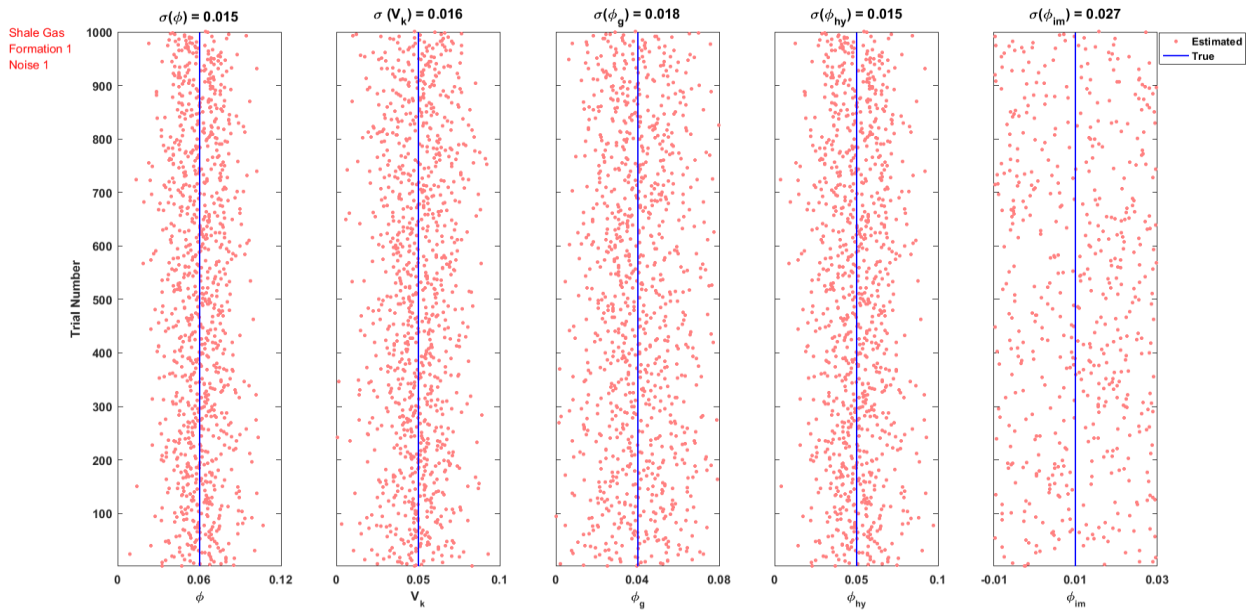

Fig. B-1—Monte Carlo simulation with abnormally high tool measurement noises in a 6-p.u. shale gas reservoir.

Fig. B-2 shows the results of a Monte Carlo simulation for a shale gas reservoir with the same reservoir properties as in the preceding simulation but with normal tool measurement noises. The results of reduced measurement noises are significant as can be seen by comparing the results in Figs. B-1 and B-2. It is noteworthy that the porosity, gas, and kerogen volumes in Fig. B-2 are predicted with standard deviations of 1.0 p.u. or less in a complex low porosity shale reservoir. These results show the importance of operators and service providers working together on pre-job planning to select logging speeds and sampling intervals that increase the measurement signal-to-noise ratios.

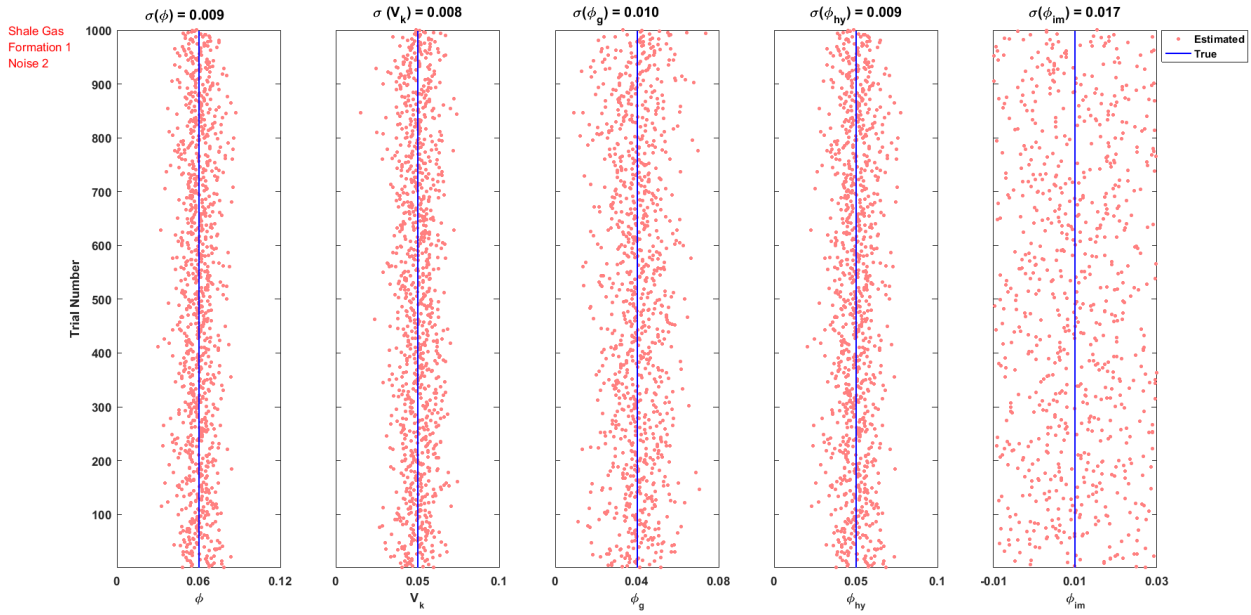

Fig. B-2—Monte Carlo simulation with normal tool measurement noises in a 6-p.u. shale gas reservoir.

The results of simulations for the 5-p.u. shale gas reservoir designated as formation 2 in Table B-1 are shown in **Figs. B-3 and B-4**. The simulations were again performed for two levels of measurement noise, and the results are qualitatively similar to those in Figs. B-1 and B-2. Observe in Fig. B-4 that for normal tool noise levels the porosity, gas volume, total hydrocarbon volume, and the kerogen volume are estimated with a standard deviation of approximately 1.0 p.u. or less.

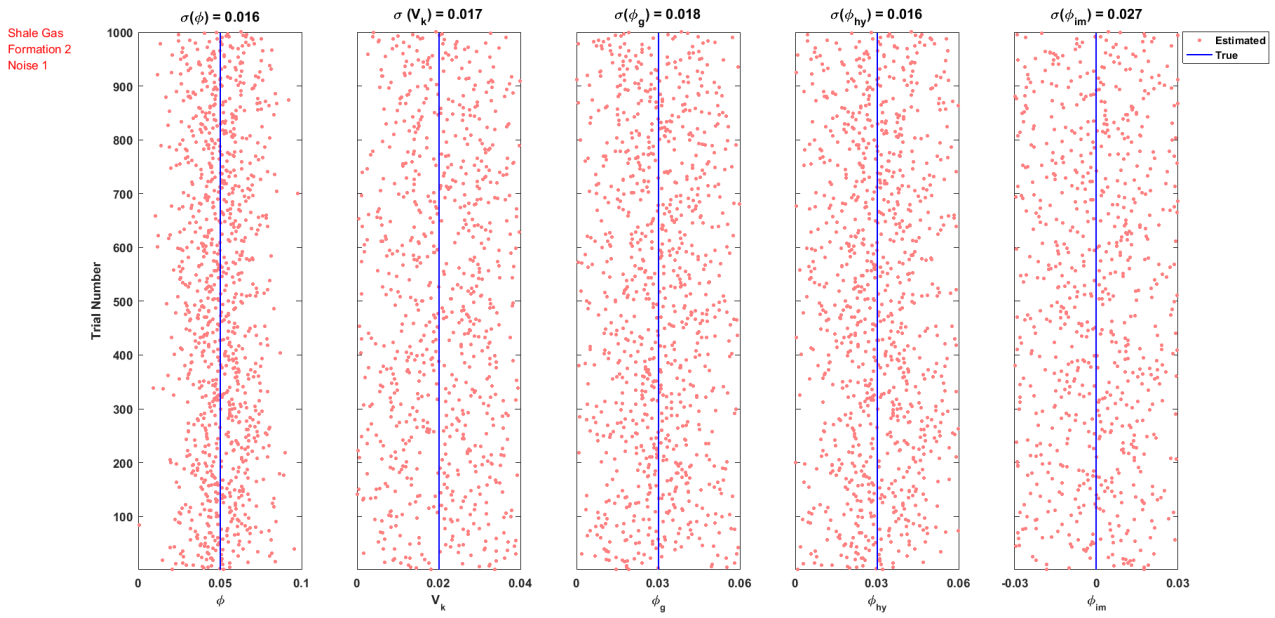

Fig. B-3—Monte Carlo simulation with abnormally high tool measurement noises in a 5-p.u. shale gas reservoir.

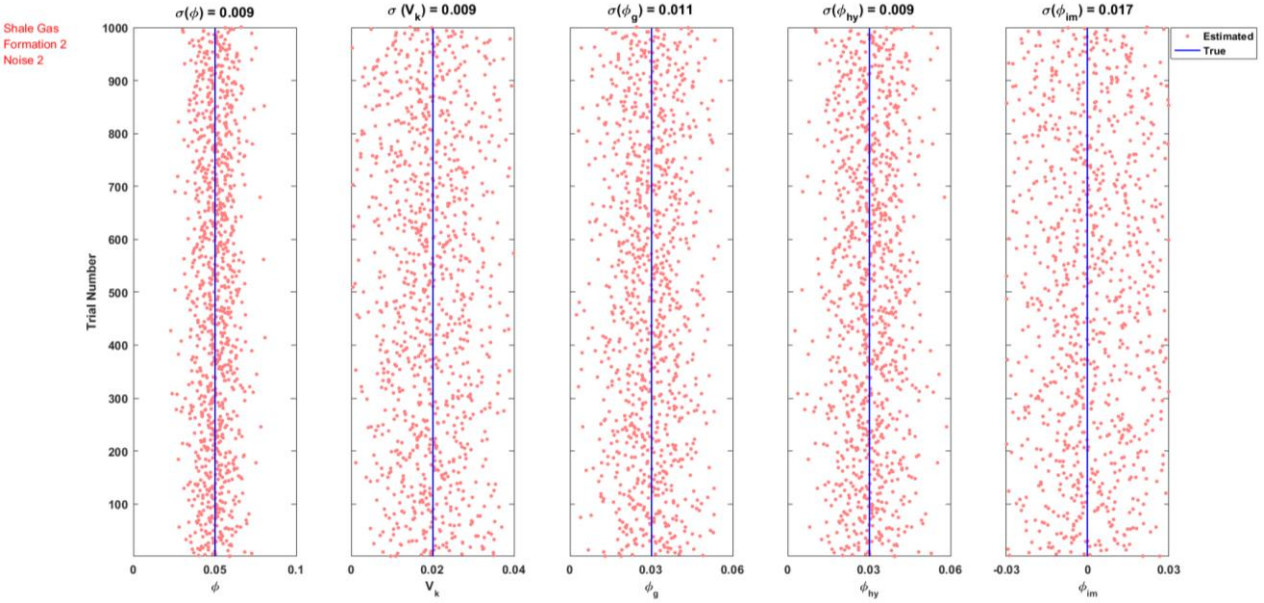

Fig. B-4—Monte Carlo simulation with normal tool measurement noises in a 5-p.u. shale gas reservoir.

Monte Carlo Simulations in Shale Tight Oil Reservoirs. This section discusses Monte Carlo simulation results for a shale tight oil reservoir for which the producible fluid is a high API gravity oil. The reservoir fluid and solid parameters used for the Monte Carlo simulations are shown in Table B-2. The same algebraic equations used to predict shale gas reservoir properties are valid for tight oil reservoirs. Many of the fluid and solid reservoir parameters often have comparable values, as can be seen, for example, by comparing the reservoir inputs in Tables B-1 and B-2. The two exceptions, however, are the higher density and HI of tight oil compared to that of gas. This reduces the light-hydrocarbon effects on the density and NMR porosity measurements. As a result, the density and NMR porosity measurements have reduced sensitivities to the volume of producible oil. The Monte Carlo simulation results for the tight oil reservoir discussed below compared to those shown above for shale gas reservoirs demonstrate that the robust estimation of producible oil volumes (ϕ_o) requires reducing measurement noise levels well below normal logging tool noise levels.

The results of a Monte Carlo tight oil simulation for the 6-p.u. formation and the reservoir fluid and solid inputs in Table B-2 are shown in **Fig. B-5** for normal tool measurement noises designated by noise 2 in Table B-3. Observe that the porosities (ϕ) and kerogen volumes (V_k) in tracks 1 and 2, respectively, are estimated with standard deviations that are both less than 1.0 p.u. Also, observe that the total hydrocarbon volumes (ϕ_{hy}) in track 4, which are the sums of the volumes of the producible oil and the immobile hydrocarbons, are predicted with precisions comparable to that of the porosity provided that the water volume estimates have reasonably low variances. On the other hand, the producible oil volumes (ϕ_o) in track 3 of Fig. B-5 have standard deviations that are almost a factor of three larger than those of the gas volumes (ϕ_g) in Fig. B-2**.** As discussed above**,** the lower precision (i.e., increased standard deviation) found for the estimated producible oil volumes is caused by the reduced sensitivity of the density porosity and NMR porosity measurements to light oil compared to gas. At this point, we can draw some general conclusions regarding the robustness of the algebraic equations in shale gas and shale oil reservoirs. The total porosity, kerogen volumes, and total hydrocarbon volumes can be estimated with comparable and good precision in both shale gas and shale tight oil reservoirs. The gas volumes in shale gas reservoirs can be estimated with good precision (about 1.0 p.u. with normal tool measurement noises). The producible oil volumes can be estimated with good precision by significantly reducing the normal tool measurement noises as shown in **Figs. B-6 and B-7**. The Monte Carlo simulation shown in Fig. B-6 was performed with a standard deviation on the NMR porosity of 0.5 p.u. (i.e., using the low tool measurement noises designated as noise level 3 in Table B-3). One sees that the standard deviation on the volume of producible oil is reduced from 3.0 p.u. to approximately 2 p.u. by reducing the noise on the NMR porosity. It should be clear that to achieve precisions on estimates of ϕ_o comparable to those that can be achieved on estimates of ϕ_g requires a significant reduction in the normal tool measurement noises. To demonstrate this, we performed a Monte Carlo simulation at "stationary logging conditions" by reducing the normal noise levels each by a factor of 5 (i.e., the very low noise levels 4 in Table B-3). The results of this simulation are shown in Fig. B-7. It is clear from Fig. B-7 that very precise volumes of producible oil can be predicted under stationary logging conditions.

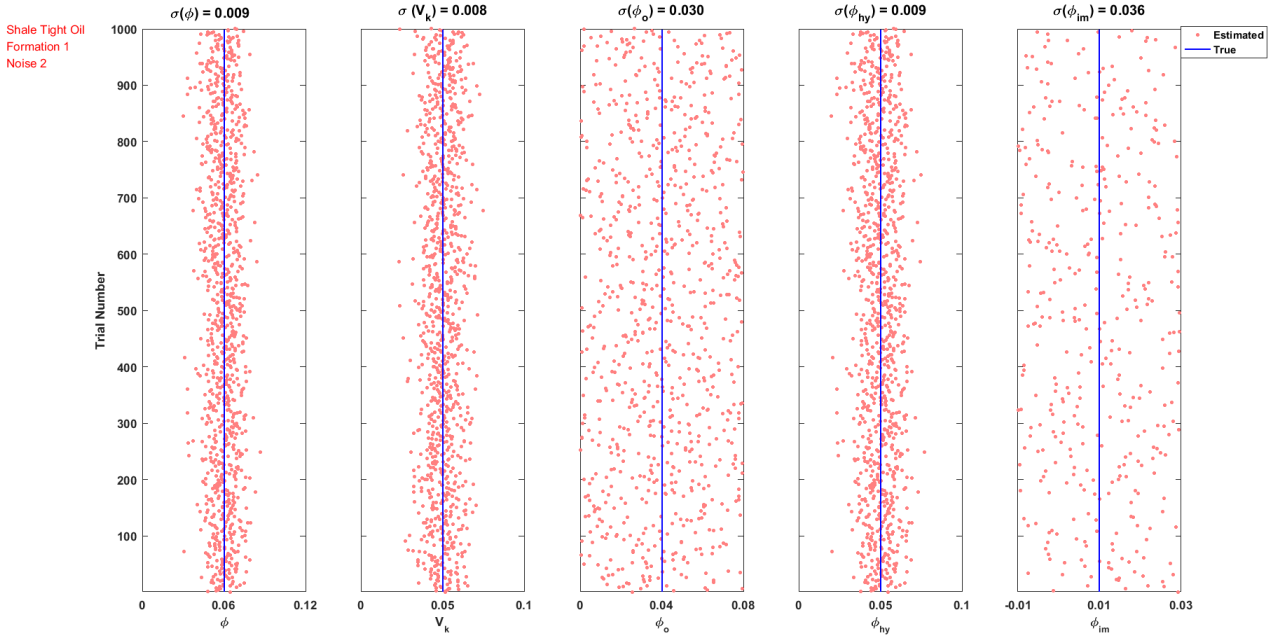

Fig. B-5—Monte Carlo simulation in a 6-p.u. shale tight oil reservoir with normal tool measurement noises.

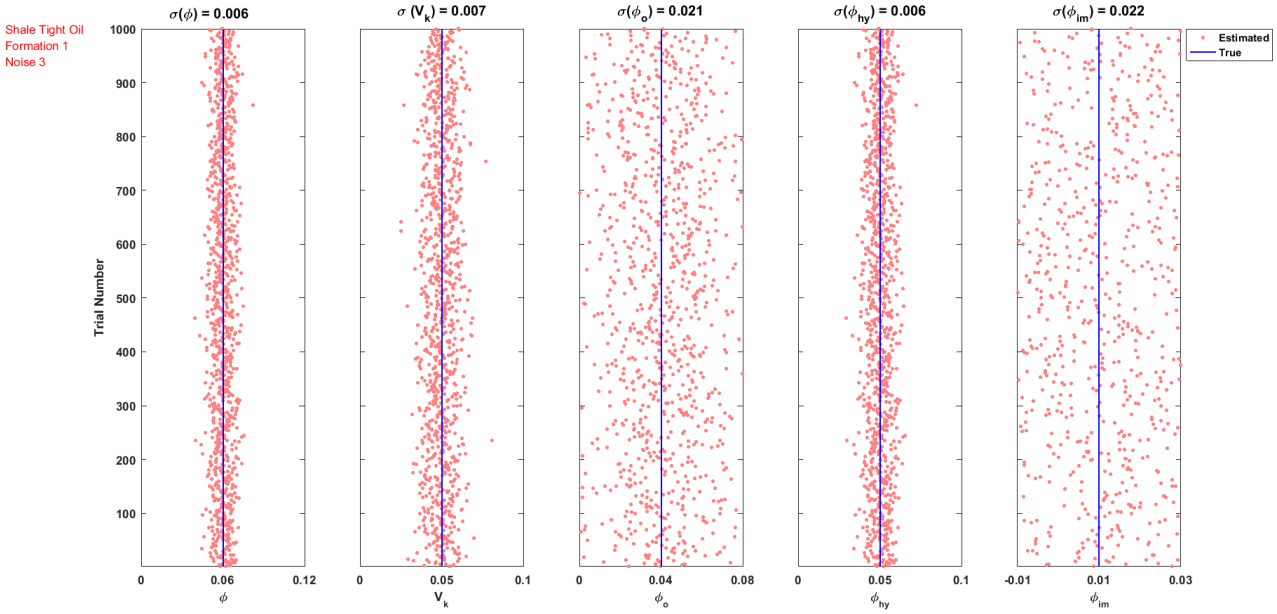

Fig. B-6—Monte Carlo simulation in a 6-p.u. shale tight oil reservoir with low tool measurement noises.

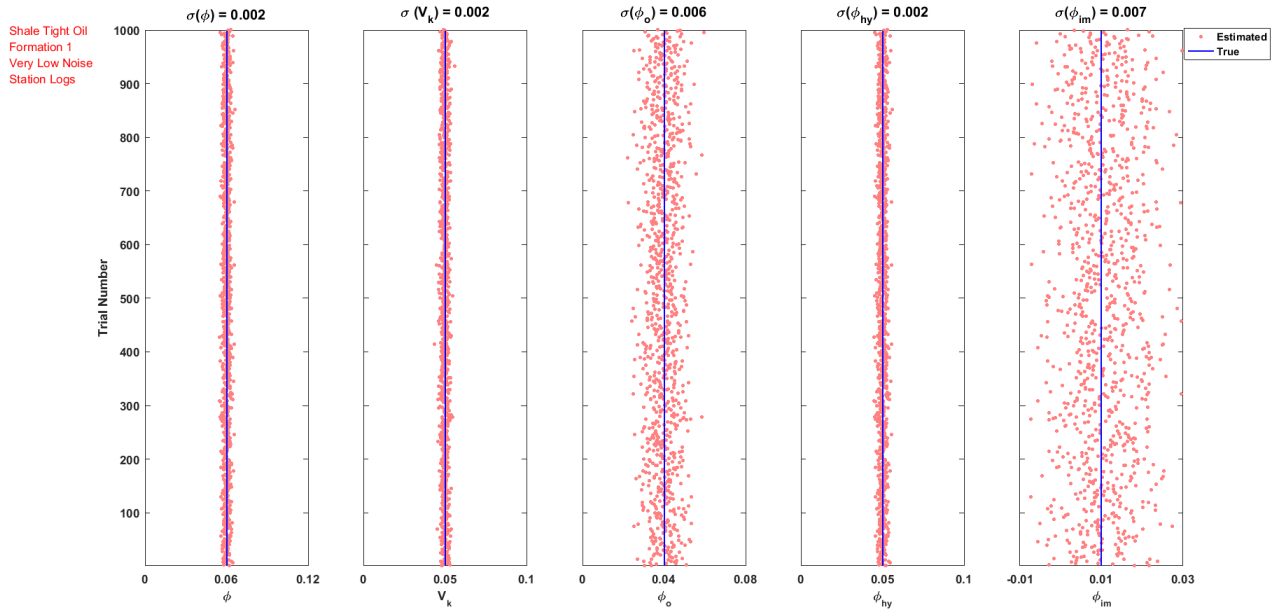

Fig. B-7—Monte Carlo simulation in a 6-p.u. shale tight oil reservoir with very low tool measurement noises that can be achieved by stationary logging.

Appendix C—Sensitivity of Solutions to Uncertainties in Reservoir Input Properties

The Monte Carlo results discussed in Appendix B are concerned with the robustness or precision of the estimated shale reservoir properties in the presence of tool measurement noises. The accuracy of the estimated results is another matter and depends on the accuracy of the reservoir inputs used for the numerous fluid and solid properties. Additionally, the accuracy depends on how well our tool response equations for organic shales represent reality, and this question cannot be answered by simulations. This question can, however, be addressed by field tests in organic reservoirs that compare predicted reservoir properties from logs with the results of core analysis. In this appendix we will discuss two examples of the effects of uncertainties in reservoir input parameters on the estimated reservoir properties. These two examples are presented here to show the magnitudes of the errors in the estimated reservoir properties that can result from these uncertainties. A full error propagation study is not attempted because a

comprehensive study would be too lengthy and would detract from the main objective of the paper, which is to introduce the new methodology.

The next two examples consider an 8-p.u. shale gas reservoir whose true reservoir properties (e.g., $\phi, \phi_g, S_g, \phi_{im}, S_{im}, \phi_w, V_k$) and true reservoir fluid and solid input properties (e.g., $c_k, c_{im}, c_g, \rho_f, \rho_g, \rho_{im}, \rho_k, HI_g, HI_f, \rho_{ma}, \phi_w$) are shown in **Table C-1**. In this example, the formation is assumed to contain bitumen and/or immobile hydrocarbons. In this case, the volume of water is an input parameter. The true reservoir properties and the true reservoir fluid and solid properties in Table C-1 can be substituted into Eqs. 1–3 to compute the tool responses. If one substitutes the tool responses and true reservoir input properties sequentially into Eqs. 12, 7, 5, and 3a, then the algebraic equations will exactly yield the true reservoir properties because the latter equations are exact solutions. However, if the tool responses, and a set of assumed reservoir inputs that differ from the true reservoir inputs, are substituted into the algebraic equations, then the estimated reservoir properties will deviate from the true reservoir properties, as expected. These deviations represent the errors in the estimated shale reservoir properties caused by uncertainties in the reservoir fluid and solid input parameters.

In Table C-1, the assumed reservoir input properties that differ from the true properties are shaded. If we then substitute the tool responses and the assumed reservoir input properties into Eqs. 12, 7, 5, and 3a, one finds the reservoir estimates shown in the last row of Table C-1. Observe that the estimated and true reservoir properties are not equal; however, the differences are relatively small and do not significantly alter the overall evaluation. The next example considers the effects of errors in ϕ_w on the predicted reservoir properties.

Reservoir Inputs	c_k	c_{im}	c_g	ρ_f	ρ_g	ρ_{im}	ρ_k	HI_g	HI_f	ρ_{ma}	ϕ_w
True Properties	0.80	0.84	0.80	1.0	0.2	1.0	1.4	0.4	1.0	2.7	1.0
Assumed Properties	0.82	0.82	0.79	1.0	0.2	1.0	1.3	0.47	1.0	2.7	1.0

Reservoir Properties	ϕ (p.u.)	ϕ_g **(p.u.)**	S_g (%)	ϕ_{im} **(p.u.)**	ϕ_w **(p.u.)**	S_{im} **(%)**	V_k **(p.u.)**
True Properties	8	6	75	1	1	12.5	3
Reservoir Estimates	7.5	5.9	78.0	0.7	NA	8.7	3.5

Table C-1—The errors in estimated reservoir properties caused by errors in the assumed reservoir fluid and solid properties. The red shaded cells show the assumed properties that differ from the true properties. The estimated reservoir properties deviate, as expected, from the true properties; however, the deviations are relatively minor, showing that the solutions are not overly sensitive to errors in the input parameters.

The example shown in **Table C-2** is similar to the one in Table C-1 except that a value of 2.5 p.u. is used as an input for ϕ_w. This increases the errors in the estimated reservoir properties as can be seen by comparing the reservoir estimates in Tables C-1 and C-2. However, the important shale gas reservoir properties are predicted with reasonable accuracy in spite of the 1.5-p.u. error in the assumed volume of water. The results in Tables C-1 and C-2 are comforting because they show that the solutions of the algebraic equations have relatively weak sensitivities to errors in the reservoir fluid and solid input parameters. The water volumes are perhaps the least well-known of the inputs and therefore the results in Table C-2 are especially encouraging. The results seen in these two examples are consistent with other sensitivity computations we have performed and also with our experience to date processing field data. As noted previously, for some mature shale gas reservoirs (e.g., Barnett shale and Marcellus shale), which do not contain bitumen or immobile oil in the area where the well is drilled, the water volume is an output instead of an input of the algebraic equations.

Reservoir Inputs	c_k	c_{im}	c_g	ρ_f	ρ_g	ρ_{im}	ρ_k	HI_g	HI_f	ρ_{ma}	ϕ_w
True Properties	0.80	0.84	0.80	1.0	0.2	1.0	1.4	0.4	1.0	2.7	1.0
Assumed Properties	0.82	0.82	0.79	1.0	0.2	1.0	1.3	0.47	1.0	2.7	2.5

Reservoir Properties	ϕ (p.u.)	ϕ_g **(p.u.)**	S_g (%)	ϕ_{im} **(p.u.)**	ϕ_w **(p.u.)**	S_{im} **(%)**	V_k **(p.u.)**
True Properties	8	6	75	1	1	12.5	3
Reservoir Estimates	7.1	5.1	71.5	0.0	NA	0.0	4.4

Table C-2**—The errors in estimated reservoir properties caused by errors in the assumed reservoir fluid and solid properties plus an error of 1.5 p.u. in the water volume. Observe that the reservoir estimates are reasonably representative of the true reservoir properties in spite of the 1.5-p.u. error in the assumed water volume.**